

# Intelligent Recognition of Gas-Liquid Two-Phase Flow Based on Optical Image

Shujuan Wang  
College of Mathematical  
Sciences, Harbin  
Engineering University,  
China  
wangshujuan@hrbeu.edu.cn

Haofu Guan  
College of Mathematical  
Sciences, Harbin Engineering  
University, China  
75753907@qq.com

Yuqing Wang  
College of Mathematical  
Sciences, Harbin Engineering  
University, China  
793429425@qq.com

Kanghui Zhang  
College of Mathematical  
Sciences, Harbin  
Engineering University,  
China  
1831231851@qq.com

Yuntao Dai\*  
College of Mathematical Sciences,  
Harbin Engineering University, China  
peach0040@126.com

Shouxu Qiao  
College of Nuclear Science and  
Technology, Harbin Engineering  
University, China  
qiaoshouxu@hrbeu.edu.cn

Jihong Shen  
College of Mathematical Sciences,  
Harbin Engineering University,  
China  
shenjihong@hrbeu.edu.cn

**Abstract:** Gas-liquid two-phase flow is widely involved in many scientific and technological fields, such as energy, electricity, nuclear energy, aerospace and environmental protection. In some fields, extracting the accurate position of bubbles in space can not only accurately capture the characteristics of bubbles in two-phase flow, but also plays an important role in the subsequent research like bubble tracking. It has got some progresses to use Convolutional Neural Network (CNNs) to identify bubbles in gas-liquid two-phase flow, while accurate pixel segmentation map in the bubble identification problem is more desirable in many areas. In this paper, VGG16-FCN model and U-Net model are utilized to identify bubbles in two-phase flow images from the perspective of semantic segmentation. LabelMe is used to label the images in the experiment, which can remove the noise in the original image. In addition, bubble pixels with low ratio relative to the background affects the loss function value tinily which cause the irrational evaluation for the recognition in traditional semantic segmentation, thus, Dice loss is used as the loss function for training to improve the recognition effect. The research results show that the two deep learning models have strong feature extraction ability and accurately detect the bubble boundary.

**Keywords:** Optical image, gas-liquid two-phase flow, machine vision, FCN, U-Net.

Received November 3, 2023; accepted October 3, 2022  
<https://doi.org/10.34028/iajit/20/4/7>

## 1. Introduction

In nature and industrial processes, multiphase flow is often involved, among which gas-liquid two-phase flow is the most common. The most basic flow form of gas-liquid two-phase flow is gas-liquid two-phase bubble flow. Bubbles participate in the enhanced mass transfer between liquid and gas phases. In addition, the bubble jet generated by some types of hydraulic equipment during operation will lead to serious consequences closely related to cavitation. Based on the importance of gas-liquid two-phase bubble flow in many fields, such as geophysics [3, 17, 39], chemical engineering [12], biopharmaceutics [23] and wastewater management [4], it is necessary to better understand the interaction between two-phase flows and especially develop high-precision methods to process and analyze two-phase flows based on the increasing experimental data [38].

There are mainly two kinds of measurement techniques for two-phase flow. the Probe-based invasive (contact) method and non-invasive (non-contact) method. The advantage of invasive is that it may use sensors to evaluate some physical quantities in

that are difficult to reach in a certain river basin. Examples are based on conductivity probe [24], impedance probes [18] and wiremesh sensors [36]. Non-invasive method includes many optical methods and computer methods, such as laser Doppler anemometer [25] and image processing technology [1, 7, 22, 26]. Since the invasive method makes the probe directly contact with the dispersed bubbles, the flow near them is disturbed, which increases the uncertainty of experimental measurement. Non-intrusive do not interfere with the flow studied and avoid most of the shortcomings of intrusive methods, so they usually show higher spatial resolution [9].

There are many traditional methods based on extracting the “manual configuration” feature to find and identify the target in the image, such as SIFT descriptors [30] or histograms of oriented gradients [14]. ImageJ analysis software was used for bubble detection and bubble size calculation of experimental images [29]. Akhmetbekov [2] proposed two bubble identification methods. The first method is to sketch the boundary of bubbles in the image, and then determine the geometric

center and size of bubbles by searching the relevant regions. The second technique uses related methods to compare the scanned image part with the pre-generated mask image, so as to determine the existence or absence of bubbles in the image. The normal operation of these two methods requires a large number of adjustable parameters. The Planar Fluorescence for Bubbles Imaging (PFBI) method [15] can be used to determine the parameters of gas-liquid two-phase flow, such as the average velocity of continuous phase, local gas concentration, flow characteristics and their fluctuations in the dispersed phase.

In recent decades, with the rapid development of computer technology and the huge growth of available data, it has become possible to use neural network for image classification or target detection and other applications [37]. Nowadays, Convolutional Neural Network (CNN) is one of the most successful examples in machine learning applications. In the classical CNN model, an image block composed of a pixel and its adjacent pixels is input into the network to extract features, and then it is used for image classification [20].

The random changes of specific location, light and environment will make it difficult to identify the target of the two-phase flow data obtained. In traditional image processing methods, feature selection is subjective and artificial, and feature extraction is not comprehensive [8]. In order to solve the above problems, CNN model with excellent performance is used in the task of visual object recognition. Poletaev *et al.* [33] compared the methods based on CNN and PFBI. The author used a sliding window method, three independent CNN to classify the probability of bubbles in some images, filtered the images through an automatic encoder, and found the possible bubble center, finally achieving superior accuracy compared with the latter. Haas *et al.* [21] proposed the use of Region based CNN (R-CNN) to identify possible bubble positions, where each bubble is identified, marked and surrounded by a rectangular box [16]. However, the CNN models in the above research use the full connection layer at its end to complete the classification task, so what they finally get is the classification probability of the input image, rather than the output semantic level pixel segmentation map. As for the bubble recognition of gas-liquid two-phase flow, the research expects more accurate image segmentation of bubbles and background, and CNN may not achieve the bubble recognition effect required in most industrial experiments [13].

In this paper, Fully Convolutional Networks (FCN) and U-Net with different fusion methods are applied to bubble identification in the field of gas-liquid two-phase flow. FCN, proposed by Shelhamer *et al.* [35], accepts images of any size as input, extracts features through convolution layer. Deconvolution upsampling is then performed to output a segmented image of the same size as the label image. At present, FCN model has been

widely used in image segmentation [5, 18, 25, 31, 32, 40]. Many subsequent image segmentation models further extend the concept of FCN. Representative models include SegNet [6], U-Net [34], DeepUNet [27], Y-Net [28] and DeepLab [10, 11].

## 2. Materials and Methods

### 2.1. Convolutional Neural Network

In Convolutional Neural Networks, both input images and feature response maps generated by convolution layer processing are usually multi-channel. A typical convolution network is composed of convolution layers, down-sampling layers and full connection layers. A convolution block is a continuous  $M$  convolution layers and  $b$  down-sampling layers. In a convolution network,  $N$  continuous convolution blocks can be stacked, and  $K$  full connection layers are connected behind. The overall structure of convolutional network is shown in Figure 1.

In convolutional neural networks, parameters are weights and biases in convolution kernels. Similar to the fully connected feedforward network, the convolutional neural network can also carry out the back propagation through the error term of each layer, and further calculate the gradient of each layer's parameters to realize the parameter learning.

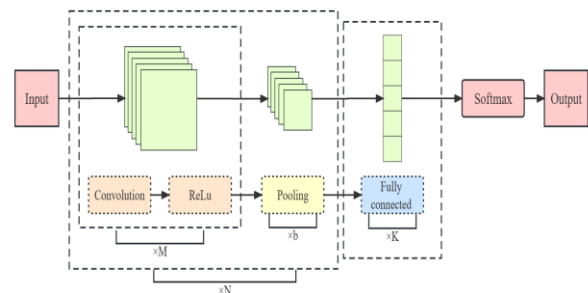


Figure 1. General structure of convolution network.

### 2.2. Feature Fusion

The purpose of image semantic segmentation technology is to label the semantic information of each pixel in the image, so as to divide the image into several regions with different properties and categories, which is a basic research content in the field of computer vision. In the feature extraction stage, a large number of down-sampling and pooling operations lead to the loss of image space and detail information, so the feature recovery and feature fusion of semantic segmentation are introduced. Feature recovery restores the resolution of the feature map by up-sampling the feature map. The commonly used up-sampling methods include bilinear interpolation and deconvolution. Feature fusion optimizes the output through the addition fusion and splicing fusion of feature maps to improve the segmentation accuracy. The two most commonly used feature fusion methods are Concat and Add.

Concat is the addition in the number of channels, and

the combination in the channel dimension (Figure 2). The advantage of Concat is that only the feature information is spliced without changing the content, thus preserving the integrity of the feature information. Concat is often used for multi-feature information fusion to increase the number of channels to maintain the integrity of information, so that network performance is greatly improved.

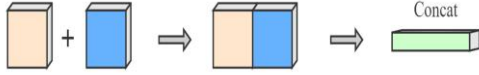


Figure 2. Concat fusion method in convolution layer.

Add is the sum of information that describes the characteristics of the image, and the number of channels is the same as the image dimension (Figure 3). This fusion method saves parameters and computation, which is also beneficial to the final image classification.

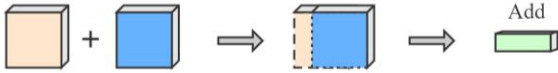


Figure 3. Add fusion method in convolution layer.

Each channel of Concat and Add corresponds to a separate convolution kernel. So the single output channel for Concat and Add are described in Equations (1) and (2) respectively.

$$Z_{concat} = \sum_{i=1}^c X_i * K_i + \sum_{i=1}^c Y_i * K_{i+c} \quad (1)$$

$$Z_{add} = \sum_{i=1}^c (X_i + Y_i) * K_i = \sum_{i=1}^c X_i * K_i + \sum_{i=1}^c Y_i * K_i \quad (2)$$

Where,  $X_i$  and  $Y_i$  are characteristic information of channel  $i$ ,  $K_i$  is convolution kernel of channel  $i$ ,  $c$  is the number of convolution kernels.

### 2.3. Loss Function and Optimizer

Dice loss training is more inclined to mining foreground regions, it can eliminate the impact of unbalanced proportions of positive and negative sample on classification results. Because the proportion of background pixels is larger than that of target bubble pixels in our experimental data, Dice loss is introduced to evaluate the identification effect in this paper.

The Dice loss formula is defined as:

$$f = 1 - \frac{2|X \cap Y|}{|X| + |Y|} \quad (3)$$

Where  $X$  and  $Y$  represent the real value and predicted value of the segmented target, respectively.  $X \cap Y$  is the intersection of  $X$  and  $Y$ . Function  $|\cdot|$  denotes the number of the set. Dice loss takes the value between 0 and 1, and the smaller the value is, the more accurate the predicted value of the model is.

In order to accelerate the training convergence speed of the model, this study selects the deep learning Adam

optimization algorithm. Compared with other optimizers, Adam optimizer is computationally efficient and suitable for large-scale data and parameter scenarios [6]. Adam Combines The Advantages Of Adaptive Gradient algorithm (AdaGrad) for sparse gradient processing and the root mean square transfer algorithm (RMSProp) for non-stationary targets. After bias correction, each iterative learning rate has a certain range, which reduces the fluctuation of parameter update and makes the model converge more smoothly [17]. The specific updates of Adam optimizer is as follow:

$$m_t = \beta_1 m_{t-1} + (1 - \beta_1) g_t \quad (4)$$

$$n_t = \beta_2 m_{t-1} + (1 - \beta_2) g_t^2 \quad (5)$$

$$\hat{m}_t = \frac{m_t}{1 - \beta_1^t}, \quad \hat{n}_t = \frac{n_t}{1 - \beta_2^t} \quad (6)$$

$$\theta_{t+1} = \theta_t - \frac{\eta}{\sqrt{\hat{n}_t} + \varepsilon} \hat{m}_t \quad (7)$$

Where,  $m_t$  and  $n_t$  are the first-order and second-order moment estimates of the gradient at time  $t$ ;  $\hat{m}_t$  and  $\hat{n}_t$  are the correction of  $m_t$  and  $n_t$  at time  $t$ ;  $\beta_1$  and  $\beta_2$  are the exponential decay rate for the 1<sup>st</sup> and 2<sup>nd</sup> moment estimates, the default values are  $\beta_1=0.9$  and  $\beta_2=0.999$   $g_t$  is gradient;  $\beta_1^t$  and  $\beta_2^t$  are the  $t$ -th power of  $\beta_1$  and  $\beta_2$ .  $\theta_{t+1}$  is the updated parameter at time  $t+1$ ;  $\eta$  is the learning rate, the default value is 0.001;  $\varepsilon = 10^{-8}$  is set to avoid taking 0 as denominator.

### 2.4. VGG16-FCN and U-Net

Different from the traditional CNN, FCN can accept any size of the input, and the feature map obtained after the last convolution layer is up-sampled by deconvolution. This operation can obtain the feature map with the same size as the original input image, which can be used for pixel-level prediction. At the same time, the spatial information in the original input image is retained to solve the problem of semantic segmentation. In this paper, based on FCN, the network structure is shown in Figure 4. The classical network VGG16 is first introduced for migration learning to remove the full connection layer, retain the convolution base part of the network, and use the pre-trained weight on the ImageNet dataset for training. Next, the core idea of semantic segmentation is introduced, namely deconvolution up-sampling and jump structure. Then, the skip fusion structure is introduced to make up for the lost features of the previous convolution layer and pooling layer. Combined with the results of different depth layers, the Add fusion method is used for upsampling and fusion.

The U-Net model was first published in MICCAI in 2015, which combines low resolution information (providing object category recognition basis) and high resolution information (providing accurate

segmentation and positioning basis). The high resolution information has an important effect on semantic segmentation and target detection. The U-Net model can not use classical convolution networks such as VGG as pre-training models, and the structure of U-Net can freely deepen the network depth according to the size of the dataset. And when U-Net performs shallow feature fusion, it uses Concat fusion. In this paper, for images of size 256\*256, four down-samplings

and four up-samplings are carried out. The feature information of the down-sampling layer is directly transmitted to the up-sampling layer of the same dimension to obtain high-resolution information, and the underlying information is filled to improve the segmentation accuracy. It can provide more fine features for semantic segmentation and target detection, and achieve accurate segmentation and recognition. The structure is shown in Figure 5.

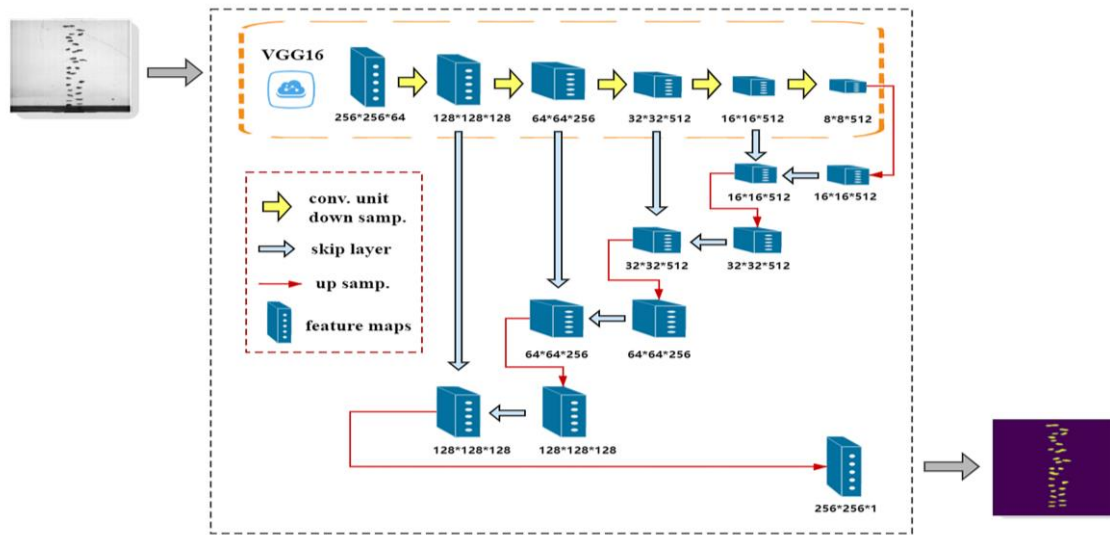


Figure 4. Structure diagram of VGG16-FCN.

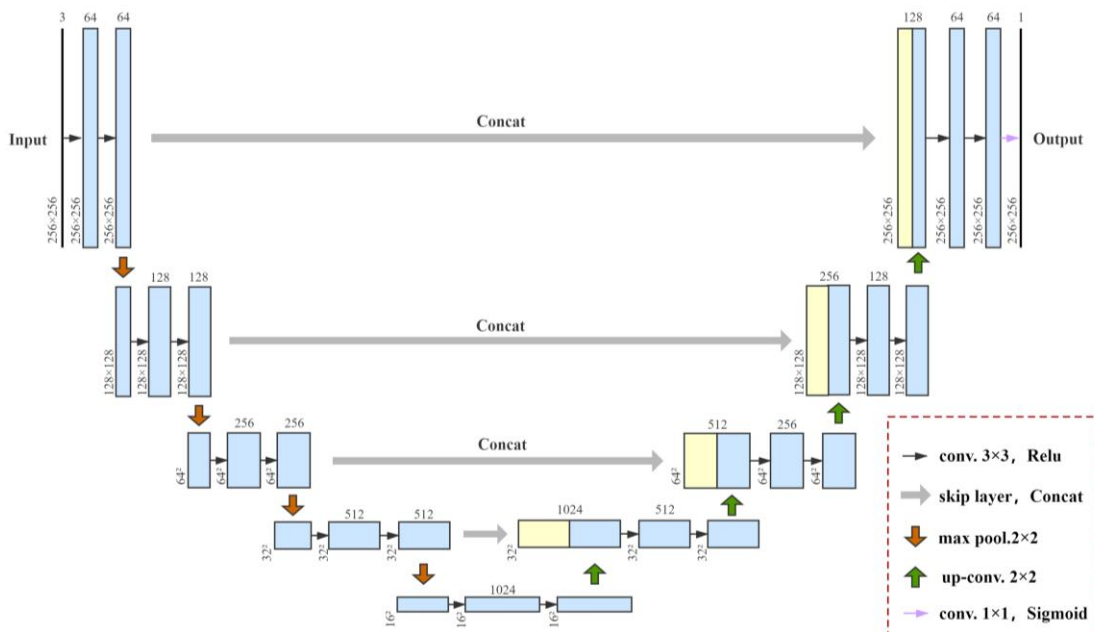


Figure 5. Structure diagram of U-Net.

### 3. Experimental Results and Discussion

#### 3.1. Hardware and Data Training

Our experiments are based on open resource deep learning frameworks TensorFlow and Theano 's Keras. Graphics Processing Unit (GPU) is NVIDIA GeForce RTX 2060, 16GB RAM. The Central Processing Unit

(CPU) is Intel Core i7-10750H, 2.60GHz. In the experiment, the initial learning rate is set to 0.001.

The data originated from the two-phase flow experiment simulated closed loop (Figure 6). By adjusting the pipeline valve, the vertical rise and down of gas-liquid two-phase flow can be controlled. For the vertical down two-phase flow, The deionized water in the water tank passes through the filter driven by the

pump, and then enters the bubble generator and the vertical test section respectively. The gas and water are separated by the gas-water separator and returned to the water tank. Using graphic design, high-speed camera can be carried out.

The image dataset of the two-phase flow contains 9351 samples obtained by intercepting each frame of the video, including. The sample size is 256\*256 pixels. In order to obtain a clear gas-liquid two-phase flow dataset, the brightness and contrast of the image were modified. And all samples were normalized by Equation (8) before used. Then, 1871 (20%) were randomly selected as test samples, and the remaining 7480 (80%) were used as training samples to train U-Net model and VGG16-FCN model.

$$image(output) = \frac{image(input) - 1}{127.5} \quad (8)$$

Where the  $image(input)$  represents the pixel value of the image sample in the interval of  $[0, 255]$ .

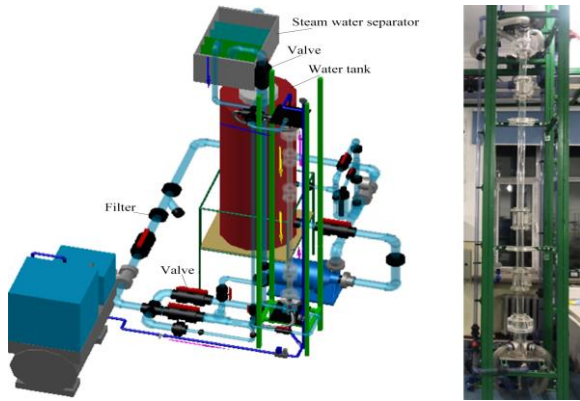


Figure 6. Two-phase flow experimental device with simulated closed loop.

### 3.2. Experimental Results and Analysis

According to the evaluation of the classification problem, Accuracy, Precision, Recall, Matthews Correlation Coefficient (MCC) and Receiver Operating Characteristic (ROC) curve are used to evaluate the accuracy of bubble identification in gas-liquid two-phase flow data set.

Accuracy:

$$accuracy = \frac{TP + TN}{TP + FP + TN + FN} \quad (9)$$

Precision and Recall:

$$precision = \frac{TP}{TP + FP} \quad (10)$$

$$recall = \frac{TP}{TP + FN} \quad (11)$$

MCC:

$$MCC = \frac{TP \times TN - TP \times FN}{\sqrt{(TP + FP) \times (TP + FN) \times (TN + FP) \times (TN + FN)}} \quad (12)$$

Where True Positive (TP) and True Negative (TN) are the the number of pixels correctly classified as bubbles

and background respectively; FP is the number of pixels wrongly classified as bubbles; False Negative (FN) is the number of pixels misclassified as background.

In general, accuracy can directly reflect the classification ability of the model for the whole sample. Precision refers to the accuracy of bubble targets detected by the system. The recall rate refers to the ratio of bubbles identified in the detection results to the total number of bubble pixels. For the binary classification problem, MCC is a comprehensive index that can comprehensively consider TP, TN, FP, and FN, especially for the model evaluation when there is a large gap between the target and the background pixel ratio, like in this experiment. One of the great advantages of ROC curve for model evaluation is that it can maintain good stability when the distribution of positive and negative samples changes. Each point on the ROC curve reflects sensitivity to the same signal stimulus. Curves plotted with True Positive Rate (TPR) as the ordinate and False Positive Rate (FPR) as the abscissa, where

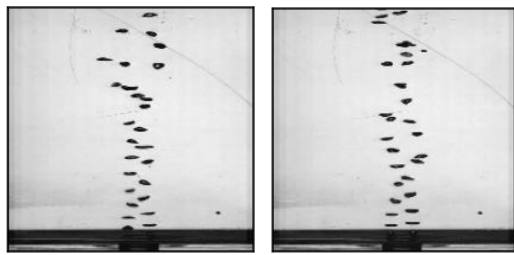
$$TPR = \frac{TP}{TP + FN}, \quad FPR = \frac{FP}{FP + TN} \quad (13)$$

The experiment is implemented with five-fold cross-validation used in model training. The experiments are conducted with batch\_size 4,8,16 respectively, and the results are shown in Table 1. It is shown that the U-Net and FCN models have a high ability to identify bubbles in data sets, and the identification accuracy of U-Net is better than that of FCN on the whole. U-Net combines shallow detail features with deep abstract features to enhance the representation of high-resolution detail information and better protect the integrity of features. It can ensure the robustness and accuracy of the image and repair the restored image.

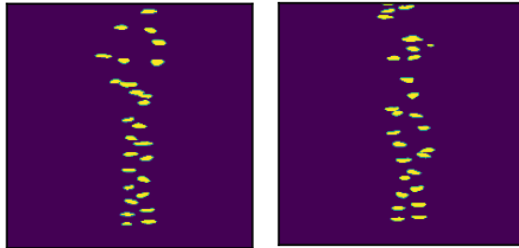
Table 1. Indicators of the training results of the two models.

Model	Batch size	Precision	Accuracy	Recall	MCC
VGG16-FCN	4	95.37 %	98.07%	95.61%	0.9535
	8	95.68 %	98.37%	96.96%	0.9593
	16	91.01 %	95.68 %	92.96 %	0.9204
U-Net	4	98.09%	99.46%	99.20%	0.9679
	8	98.18%	99.47%	99.81%	0.9788
	16	96.87%	98.34%	96.55%	0.9574

Figures 7 and 8 show the performance of the FCN model and U-Net with batch\_size 8 when the identification accuracy is the highest. In this condition, the accuracy of U-Net model can reach 99.47 %, and the accuracy of FCN can reach 98.37 %. The ROC curve of U-Net model is shown in Figure 9, the six data points are calculated by TPR and FPR after the thresholds are selected by equal distance. The Area Under The Curve (AUC) is close to 1, indicating that the U-Net model has a good classification effect.

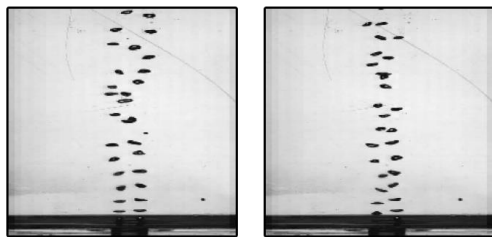


a) Original figure.

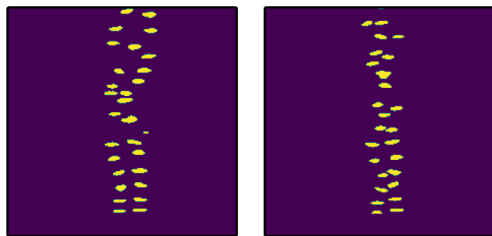


b) The image after semantic segmentation.

Figure 7. Identification results of bubbles by FCN model.



a) Original figure.



b) The image after semantic segmentation.

Figure 8. Identification results of bubbles by U-Net model.

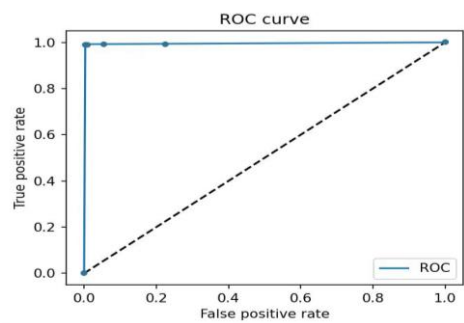
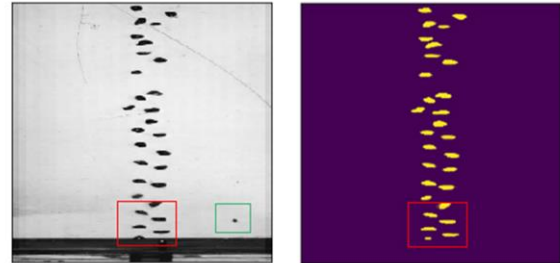


Figure 9. ROC curve of U-Net network.

Through experiments, we also found that the two models can not only identify complete bubbles well, but also has a good recognition effect for bubbles that have just been generated (Figure 10) and bubbles that are about to surface (Figure 11). The bubble diagrams in both cases are circled with red boxes. The green box circled in the Figures 10 and 11 is a bubble-like particle

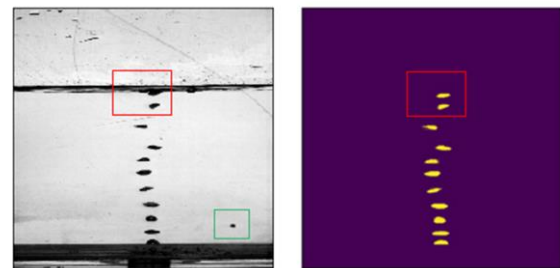
on the outer wall of the experimental instrument in this experiment. The two networks used in this paper did not recognize the bubbly particles as bubbles, so they can well adapt to the experimental equipment and environment, and distinguish bubbles from other underwater particles and noises.



a) Original figure.

b) Identification result of bubbles.

Figure 10. The original image and the identification result of bubbles that have just been generated.



a) Original figure.

b) Identification result of bubbles.

Figure 11. The original image and the identification result of bubbles floating out of water.

### 3.3. Discussion

Aiming at the bubble identification problem when the target bubble pixel is annihilated by the background pixel in the gas-liquid two-phase flow, VGG16-FCN model and U-Net model based on semantic segmentation are used in this paper. The method of semantic segmentation, not like that in the field of classical image recognition which only gives rough ellipsoidal labels, accurately distinguishes the bubble edge from the background to form a binary recognition result. To improve the accuracy of bubble recognition, Dice loss is proposed as the loss function of the network to solve the problem that the background pixel ratio is much larger than the target bubble ratio, and the recognition accuracy of the network has been greatly improved.

In the comparative experiments, by setting different batch\_size, the Accuracy, Precision, Recall and MCC of the U-Net and VGG16-FCN deep learning models are listed in Table 1 to show the performance. It is believed that these two models perform well in the information extraction of closed-loop simulation experiments. The lowest accuracy of the two models is 95.68 % and 98.34% respectively when the parameter batch\_size is 16, and the accuracy of both models reaches the highest value at the same time when batch\_size is 8. For U-Net model, the ROC curve plots the TPR against the FPR by

varying a threshold in Figure 9, which illustrates the diagnostic ability of a binary classification system, and large area (be close to 1) under the curve indicates good performance.

#### 4. Conclusions

In this paper, we use VGG16-FCN and U-Net models to accurately identify bubbles in two-phase flow images obtained by simulating closed loop experiments. When the background pixel ratio is high and the cross entropy loss function cannot accurately segment the image, Dice loss is used as the loss function of the model. The networks are trained on this dataset and the experimental results are compared. The experimental results show that the two models used in this paper has certain robustness and anti-noise ability, and has good application value in the field of bubble identification.

Determining the spatial location, size and distribution of bubbles has always been an area of interest to researchers. The gas-liquid two-phase flow identification method based on deep learning models proposed in this paper can also be applied to the problem that the proportion of target pixels is far less than that of background pixels, as well as in subsequent fields such as bubble tracking. In the samples of this experiment, there are single-row and double-row bubble flows, and their distribution trends are basically the same, showing a linear distribution. However, in practical application scenarios, there will be more complex bubble distribution in the sample, and more noise or object occlusion will interfere with bubble recognition. Therefore, in the subsequent work, it is necessary to identify the samples with more interference factors and dense bubbles in the field of gas-liquid two-phase flow identification.

#### 5. Acknowledgements

This work was supported by the Fundamental Research Funds for the Central universities with the number of 3072022CFJ2403, 3072022JC2401 and 3072020CFT0104, and the eighth Research Institute of China Aerospace Science and Technology Corporation.

#### References

- [1] Acuña C. and Finch J., "Tracking Velocity of Multiple Bubbles in A Swarm," *International Journal of Mineral Processing*, vol. 94, no. 3-4, pp. 147-158, 2010. <https://doi.org/10.1016/j.minpro.2010.02.001>
- [2] Akhmetbekov Y., Alekseenko S., and Dulin V., "Planar Fluorescence for Round Bubble Imaging And its Application for the Study of an Axisymmetric Two-Phase Jet," *Experiments in Fluids*, vol. 48, no. 4, pp. 615-629, 2010. <https://doi.org/10.1007/s00348-009-0797-0>
- [3] Asher W., Karle L., and Higgins B., "The Influence of Bubble Plumes on Air Seawater Gas Transfer Velocities," *Journal of Geophysical Research*, vol. 101, no. C5, pp. 12027-12041, 1996. <https://doi.org/10.1029/96JC00121>
- [4] Asselin C., Comeau Y., and Ton-That Q., "Alpha Correction Factors for Static Aerators and Fine Bubble Diffusers Used in Municipal Facultative Aerated Lagoons," *Water Science and Technology*, vol. 38, no. 3, pp. 79-85, 1998. [https://doi.org/10.1016/S0273-1223\(98\)00555-1](https://doi.org/10.1016/S0273-1223(98)00555-1)
- [5] Audebert N., Saux B., and Lefèvre S., "Semantic Segmentation of Earth Observation Data Using Multimodal and Multi-scale Deep Networks," in *Proceeding of Asian Conference on Computer Vision*, pp. 180-196, 2016. <https://doi.org/10.48550/arXiv.1609.06846>
- [6] Badrinarayanan V., Kendall A., and Cipolla R., "SegNet: A Deep Convolutional Encoder Decoder Architecture for Scene Segmentation," *IEEE Trans Pattern Anal Mach Intell*, vol. 39, no. 12, pp. 2481-2495, 2017. DOI: [10.1109/TPAMI.2016.2644615](https://doi.org/10.1109/TPAMI.2016.2644615)
- [7] Cerqueira R., Paladino E., Ynumaru B., and Maliska C., "Image Processing Techniques for the Measurement of Two-Phase Bubbly Pipe Flows using Particle Image and Tracking Velocimetry (PIV/PTV)," *Chemical Engineering Science*, vol. 189, pp. 1-23, 2018. <https://doi.org/10.1016/j.ces.2018.05.029>
- [8] Cerqueira R. and Paladino E., "Development of A Deep Learning-Based Image Processing Technique for Bubble Pattern Recognition and Shape Reconstruction in Dense Bubbly Flows," *Chemical Engineering Science*, vol. 230, pp. 116163, 2021. <https://doi.org/10.1016/j.ces.2020.116163>
- [9] Chen G., Li C., Wei W., and Jing W., "Fully Convolutional Neural Network with Augmented Atrous Spatial Pyramid Pool and Fully Connected Fusion Path for High Resolution Remote Sensing Image Segmentation," *Applied Sciences*, vol. 9, no. 9, pp. 1-14, 2019. <https://doi.org/10.3390/app9091816>
- [10] Chen L., Papandreou G., Kokkinos I., Murphy K., and Yuille A., "DeepLab: Semantic Image Segmentation with Deep Convolutional Nets, Atrous Convolution, and Fully Connected CRFs," *IEEE Transactions on Pattern Analysis and Machine Intelligence*, vol. 40, no. 4, pp. 834-848, 2016. DOI: [10.1109/TPAMI.2017.2699184](https://doi.org/10.1109/TPAMI.2017.2699184)
- [11] Chen L., Papandreou G., Schroff F., and Hartwig A., "Rethinking Atrous Convolution for Semantic Image Segmentation," *arXiv preprint*, 2017. [10.48550/arXiv.1706.05587](https://arxiv.org/abs/1706.05587)
- [12] Clift R., Grace J., and Weber M., *Bubbles, Drops, and Particles*, Courier Corporation, 1978. <https://doi.org/10.1016/j.cej.2022.137859>
- [13] Cui Y., Li C., Zhang W., Ning X., Shi X., Gao J.,

- and Lan X., "A Deep Learning-Based Image Processing Method for Bubble Detection, Segmentation, and Shape Reconstruction in High Gas Holdup Sub-Millimeter Bubbly Flows," *Chemical Engineering Journal*, vol. 449, pp. 137859, 2022. <https://doi.org/10.1016/j.cej.2022.137859>
- [14] Dalal N. and Triggs B., "Histograms of Oriented Gradients for Human Detection," in *Proceedings of the IEEE Computer Society Conference on Computer Vision and Pattern Recognition*, San Diego, pp. 886-893, 2005. DOI: [10.1109/CVPR.2005.177](https://doi.org/10.1109/CVPR.2005.177)
- [15] Dulin V., Markovich D., and Pervunin K., "The Optical Principles of PFBI Approach," *AIP Conference Proceedings*, vol. 1428, pp. 1, 2012. <https://doi.org/10.1063/1.3694709>
- [16] Elumalai G., and Ganesan M., "Deep Learning Based Hand Wrist Segmentation using Mask R-CNN," *The International Arab Journal of Information Technology*, vol. 19, no.5, pp. 785-792, 2022. <https://iajit.org/portal/images/Year2022/No.5/19843.pdf>
- [17] Farmer D., McNeil C., and Johnson B., "Evidence for the Importance of Bubbles in Increasing Air-Sea Gas Flux," *Nature*, vol. 361, no. 18, pp. 620-623, 1993. [10.1038/361620a0](https://doi.org/10.1038/361620a0)
- [18] Fu G., Liu C., Zhou R., Sun T., and Zhang Q., "Classification for High Resolution Remote Sensing Imagery Using a Fully Convolutional Network," *Remote Sens*, vol. 9, no. 5, pp. 498, 2017. <https://doi.org/10.3390/rs9050498>
- [19] Garnier C., Lance M., and Marié J., "Measurement of Local Flow Characteristics in Buoyancy Driven Bubbly Flow At High Void Fraction," *Experimental Thermal and Fluid Science*, vol. 26, no. 6-7, pp. 811-815, 2002. [https://doi.org/10.1016/S0894-1777\(02\)00198-X](https://doi.org/10.1016/S0894-1777(02)00198-X)
- [20] Guo Z., Shao X., Xu Y., Miyazaki H., Ohira W., and Shibasaki R., "Identification of Village Building via Google Earth Images and Supervised Machine Learning Methods," *Remote Sens*, vol. 8, no. 4, pp. 271, 2016. <https://doi.org/10.3390/rs8040271>
- [21] Haas T., Schubert C., Eickhoff M., and Pfeifer H., "Bubcnn: Bubble Detection Using Faster RCNN and Shape Regression Network," *Chemical Engineering Science*, vol. 216, pp. 115467, 2020. <https://doi.org/10.1016/j.ces.2019.115467>
- [22] Karn A., Ellis C., Arndt R., and Hong J., "An Integrative Image Measurement Technique for Dense Bubbly Flows with A Wide Size Distribution," *Chemical Engineering Science*, vol. 122, pp. 240-249, 2015. <https://doi.org/10.1016/j.ces.2014.09.036>
- [23] Kawase Y., Halard B., and Moo-Young M., "Liquid Phase Mass Transfer Coefficients in Bioreactors," *Biotechnology and Bioengineering*, vol. 39, no. 11, pp. 1133-1140, 1992. DOI: [10.1002/bit.260391109](https://doi.org/10.1002/bit.260391109)
- [24] Kim S., Fu X., Wang X., and Ishii M., "Development of the Miniaturized Four-Sensor Conductivity Probe and The Signal Processing Scheme," *International Journal of Heat and Mass Transfer*, vol. 43, no. 22, pp. 4101-4118, 2000. [https://doi.org/10.1016/S0017-9310\(00\)00046-6](https://doi.org/10.1016/S0017-9310(00)00046-6)
- [25] Kulikajevs A., Maskeliūnas R., Damaševičius R., and Misra S., "Reconstruction of 3D Object Shape Using Hybrid Modular Neural Network Architecture Trained on 3D Models from ShapeNetCore Dataset," *Sensors(Basel)*, vol. 19, no. 7, pp. 1553, 2019. [10.3390/s19071553](https://doi.org/10.3390/s19071553)
- [26] Lau Y., Deen N., and Kuipers J., "Development of an Image Measurement Technique for Size Distribution in Dense Bubbly Flows," *Chemical Engineering Science*, vol. 94, pp. 20-29, 2013. <https://doi.org/10.1016/j.ces.2013.02.043>
- [27] Li R., Liu W., Yang L., Sun S., Hu W., Zhang F., and Li W., "Deepunet: A Deep Fully Convolutional Network for Pixel-Level Sea-Land Segmentation," *IEEE J Sel Top Appl Earth Observ Remote Sens*, vol. 11, no. 11, pp. 3954-3962, 2018. DOI: [10.1109/JSTARS.2018.2833382](https://doi.org/10.1109/JSTARS.2018.2833382)
- [28] Li Y., Xu L., Rao J., Guo L., Yan Z., and Jin S., "A Y-Net Deep Learning Method for Road Segmentation Using High-Resolution Visible Remote Sensing Images," *Remote Sensing Letters*, vol. 10, no. 4, pp. 381-390, 2019. <https://doi.org/10.1080/2150704X.2018.1557791>
- [29] Liu Z., Qi F., Li B., and Cheung S., "Modeling of Bubble Behaviors And Size Distribution in A Slab Continuous Casting Mold," *International Journal of Multiphase Flow*, vol. 79, pp. 190- 201, 2016. <https://doi.org/10.1016/j.ijmultiphaseflow.2015.07.009>
- [30] Lowe D., "Distinctive Image Features from Scale-Invariant Keypoints," *International Journal of Computer Vision*, vol. 60, pp. 91-110, 2004. <https://doi.org/10.1023/B:VISI.0000029664.99615.94>
- [31] Maggiori E., Tarabalka Y., Charpiat G., and Alliez P., "Convolutional Neural Networks for Large-Scale Remote Sensing Image Classification," *IEEE Transactions on Geoscience and Remote Sensing*, vol. 55, pp. 645-657, 2016. DOI: [10.1109/TGRS.2016.2612821](https://doi.org/10.1109/TGRS.2016.2612821)
- [32] Mboga N., Georganos S., Grippa T., Lennert M., Vanhuyse S., and Wolff E., "Fully Convolutional Networks and Geographic Object-Based Image Analysis for the Classification of VHR Imagery," *Remote Sensing*, vol. 11, no. 5, pp. 597, 2019. [10.3390/rs11050597](https://doi.org/10.3390/rs11050597)
- [33] Poletaev I., Tokarev M., and Pervunin K., "Bubble Patterns Recognition using Neural Networks: Application to The Analysis of A Two-Phase

Bubbly Jet,” *International Journal of Multiphase Flow*, vol. 126, pp. 103194, 2020. <https://doi.org/10.1016/j.ijmultiphaseflow.2019.103194>

- [34] Ronneberger O., Fischer P., and Brox T., “U-Net: Convolutional Networks for Biomedical Image Segmentation,” in *Proceedings of the International Conference on Medical Image Computing and Computer-Assisted Intervention*, Munich, pp. 234-241, 2015.
- [35] Shelhamer E., Long J., and Darrell T., “Fully Convolutional Networks for Semantic Segmentation,” *IEEE Transactions on Pattern Analysis and Machine Intelligence*, vol. 39, pp. 640-651, 2017. DOI: [10.1109/TPAMI.2016.2572683](https://doi.org/10.1109/TPAMI.2016.2572683)
- [36] Simonnet M., Gentric C., Olmos E., and Midoux N., “Experimental Determination of the Drag Coefficient in A Swarm of Bubbles,” *Chemical Engineering Science*, vol. 62, pp. 858-866, 2007. <https://doi.org/10.1016/j.ces.2006.10.012>
- [37] Szegedy C., Toshev A., and Erhan D., “Deep Neural Networks for Object Detection,” *Advances in Neural Information Processing Systems and Curran Associates Inc*, vol. 26, pp. 2553-2561, 2013.
- [38] Wen D., Chen W., Yin J., Song Y., Ren M., and Wang D., “Overlapping Bubble Detection and Tracking Method Based on Convolutional Neural Network and Kalman Filter,” *Chemical Engineering Science*, vol. 263, pp. 118059, 2022. <https://doi.org/10.1016/j.ces.2022.118059>
- [39] Woolf D., *Bubbles and Their Role in Gas Exchange*, Cambridge: Cambridge University Press, 1997.
- [40] Yuan J., “Automatic Building Extraction in Aerial Scenes Using Convolutional Networks,” *arXiv preprint*, 2016. <https://doi.org/10.48550/arXiv.1602.06564>



**Shujuan Wang** completed her B.Sc. degree in Mathematics and applied mathematics, M.Sc degree and Ph.D at Harbin Engineering University. She is currently a faculty member and associate professor at Harbin Engineering University. Her interest research field are complex system analysis and modelling, Signal processing, and Artificial intelligence.



**Haofu Guan** completed his bachelor's degree at Harbin University of Science and Technology, and pursued a master's degree in mathematics at Harbin Engineering University since 2020, His research interests are artificial intelligence and data analysis.



analysis.

**Yuqing Wang** completed a bachelor's degree at Changchun University of Technology, and a master's degree in mathematics at Harbin Engineering University since 2020, with research interests in artificial intelligence and data



optimization.

**Kanghui Zhang** completed her bachelor's degree in mathematics and applied mathematics and has been studying for a master's degree in mathematics at Harbin Engineering University since 2020. Her area of interest is artificial intelligence and



research interests are swarm intelligent, machine learning and image processing.

**Yuntao Dai** completed her Ph.D. in System Engineering at Harbin Engineering University. she is currently a faculty member and associate professor at the College of Mathematical Sciences, Harbin Engineering University. Her main



interests include thermal-hydraulics and reactor safety, two-phase flow experiments and modeling, interfacial area transport modeling.

**Shouxu Qiao** complicated his Ph. D. degree in Nuclear Engineering at The Pennsylvania State University. He is currently a faculty member and associate professor of Nuclear Science and Technology, Harbin Engineering University. His research



School of Mathematical Sciences and Professor at Harbin Engineering University. Research areas include computational mathematics, applied mathematics and operations research and control, optimization algorithms and system modeling.

**Jihong Shen** completed his B.Sc. degree in Mathematics and applied mathematics and M.Sc degree at Jilin University, and completed her Ph.D. in System Engineering at Harbin Engineering University. He is currently a faculty Dean of the